

Y₂O₂S : Eu³⁺ nanocrystals—synthesis and luminescent properties**J. Dhanaraj, R. Jagannathan* and D. C. Trivedi**Central Electrochemical Research Institute, Karaikudi 630006 (T.N), India.
E-mail: jags57_99@yahoo.com

Received 21st February 2003, Accepted 8th May 2003

First published as an Advance Article on the web 23rd May 2003

Luminescent Y₂O₂S : Eu³⁺ nanoceramics having an average particle size of 20 nm has been prepared through a gel–polymer thermolysis process employing a urea–formaldehyde resin. In this nanocrystalline system, large blue shifts (in relation to the bulk system) of ~5000 cm⁻¹ and ~2000 cm⁻¹ in the photoluminescence excitation bands corresponding to the excitonic region and the Eu³⁺–ligand charge transfer region respectively have been observed. These may be explained by considering possible size dependent changes in optical electronegativity and quantum confinement effects occurring in this large bandgap semiconductor system.

1. Introduction

Rare-earth doped luminescent nanoceramics having interesting opto-electronic properties attract a great deal of interest from material chemists.^{1,2} Considering the pronounced difference in the exciton–lattice interaction behaviour,^{3–6} these nanoceramics can be classified into two classes, *viz.* semiconductor type, *e.g.* ZnS, CdS/Se, and insulator type, *e.g.* Y₂O₃ : Eu³⁺, Y₃Al₅O₁₂ : Ce³⁺. Lanthanide doped oxysulfides are extensively applied in industry as phosphors for color television picture tubes and storage phosphors for radiographic imaging.^{7,8} Lanthanide doped oxysulfides, especially Y₂O₂S : Eu³⁺, find applications in field emission display (FED) devices.^{9,10}

The yttrium oxysulfide system having a bandgap of about 4.6 eV can be classified as a large bandgap semiconductor system.¹¹ Hence the oxysulfide nanostructure, apart from its applications, might constitute an interesting system for fundamental studies. In this investigation we have synthesized Y₂O₂S : Eu³⁺ nanocrystals using a novel sol–gel polymer thermolysis route. The salient feature of the present work is the synthesis of nanocrystalline Y₂O₂S : Eu³⁺ using a urea–formaldehyde resin (UFR) and as far as we are aware there are no reports using UFR for the synthesis of any ceramic ultra-fine particles. We present results related to the synthesis of Y₂O₂S : Eu³⁺ nanocrystals and also the photoluminescence properties of the nanocrystalline Y₂O₂S : Eu³⁺ system. Interestingly for optical excitations near the band-edge of the host matrix, the less covalent Y₂O₂S : Eu³⁺ nanocrystals seem to exhibit pronounced surface states *versus* exciton interaction properties when compared with the covalent Y₂O₃ : Eu³⁺ nanocrystals.

2. Experimental

The synthesis of nanocrystalline Y₂O₂S : Eu³⁺ (also Y₂O₃ : Eu³⁺) is schematically illustrated in Fig. 1. The urea–formaldehyde resin network can serve both as a fuel and as a dispersing medium. The urea–formaldehyde resin used in this investigation was prepared conventionally by the addition of urea and formaldehyde in the molar ratio 1 : 2 resulting in a condensation reaction of urea and formaldehyde.¹² The fuel added was in accordance with the calculation making use of the total oxidizing and reducing valencies (represented as ‘+’ and ‘-’ valencies) of the components that serve as numerical coefficients for the stoichiometric balance so that the equivalence ratio is maintained as unity for the energy released by the combustion to be maximum.¹³ When using urea as the fuel, the valency was calculated to be 6+ and for Y(NO₃)₃ it was calculated to be 15-. Thus the stoichiometry for the preparation

of Y₂O₃ (+Eu₂O₃) from Y(NO₃)₃: urea is 1 : 2.5. For the present synthesis, the amount of urea added was calculated as indicated above.

A mixed Y/Eu(NO₃)₃ stock solution was prepared using 2.429 × 10⁻³ M Y(NO₃)₃ and 1.847 × 10⁻⁴ M Eu(NO₃)₃ solutions obtained from the corresponding oxides (of 99.9% purity as obtained from Indian Rare Earths) by dissolution in nitric acid (Analyzed Reagent). To 10 ml of this solution 6.6667 × 10⁻³ M urea and 0.0147 M formaldehyde solution were added followed by the addition of 0.03125 M sulfur (Analyzed Reagent). In order to accelerate the polymerization process and also to evaporate off the excess water, the mixture was heated at 60 °C. The solidified mass thus obtained was

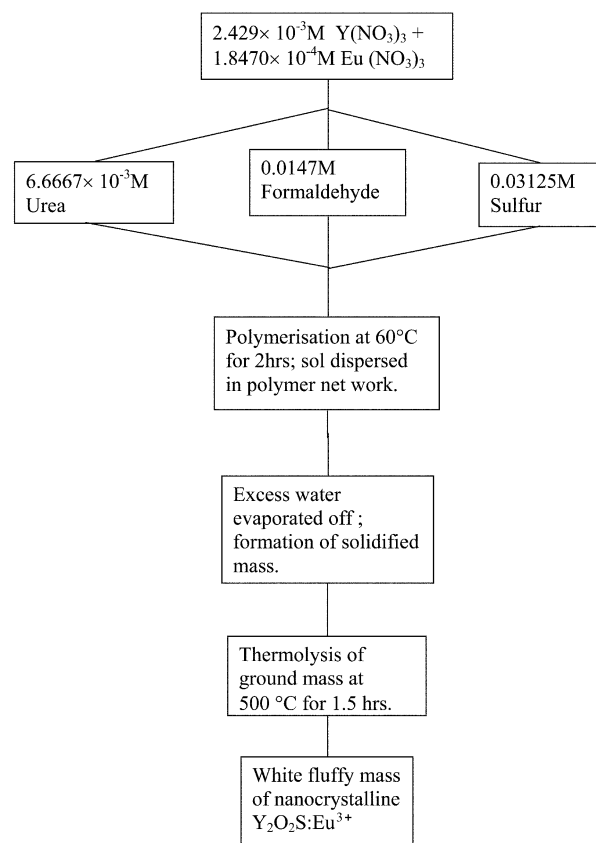


Fig. 1 Flow chart illustrating the preparation of nanocrystalline Y₂O₂S : Eu³⁺.

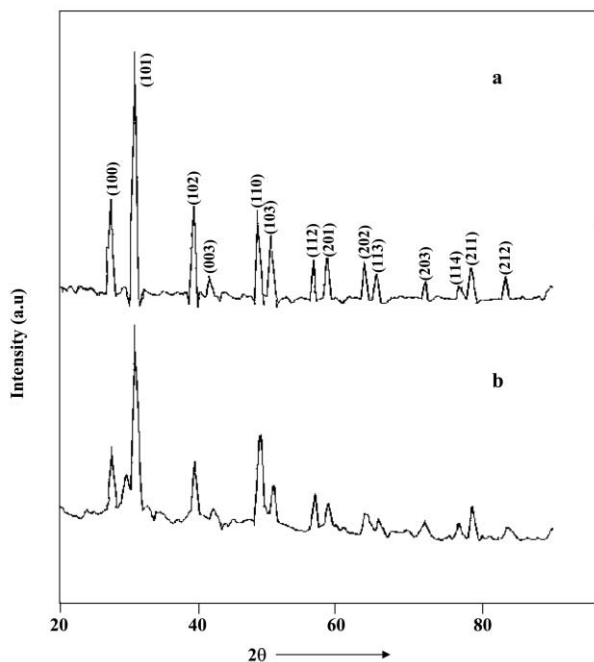


Fig. 2 X-Ray diffraction patterns (using CuK α at $T = 300$ K) for $Y_2O_2S : Eu^{3+}$: (a) bulk standard sample, (b) nanocrystalline sample.

thoroughly ground and thermolysed at 500 °C for 1.5 h in sulfur atmosphere. The product thus obtained from this combustion reaction was a white fluffy mass. For comparison purposes nanocrystalline samples of $Y_2O_3 : Eu^{3+}$ were prepared by following the above procedure without the addition of sulfur. The samples thus prepared were not further surface treated and all of the measurements were made within an hour of the sample preparation. For comparison purposes, a bulk $Y_2O_2S : Eu^{3+}$ sample having an average particle size of 2–5 μm was prepared by the conventional sulfide fusion method.¹⁴

The samples were examined for their chemical phase purity using X-ray powder diffraction (XRD) analysis (JEOL 8030 employing CuK α radiation). An estimate of crystallite size for the nanocrystalline samples was carried out using XRD line-broadening data in conjunction with Scherrer formula.¹⁵ A Hitachi H-7100 transmission electron microscope (TEM) was used to record the images of the particles and selected area electron diffraction pattern of the nanocrystalline samples. The other experimental details pertaining to photoluminescence studies were the same as described before.¹⁶

3. Results and discussion

3.1. $Y_2O_2S : Eu^{3+}$ nanocrystal synthesis

In the conventional sulfide-fusion method employed for the synthesis of micron sized bulk Y_2O_2S particles, sulfurization takes place over the surface of Y_2O_3 crystallites.¹⁷ The same analogy seems to apply for the Y_2O_2S nanocrystal synthesis employed in the present investigation. Also in this sol–gel polymer thermolysis process, Y_2O_3 particles serve as nucleating centers. Sulfurization occurs through a gas–solid phase interaction between Y_2O_3 (and Eu_2O_3) solid particles and ammonium

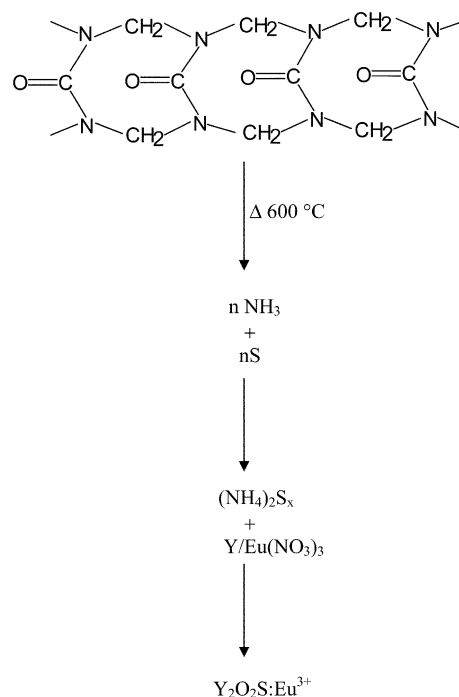


Fig. 3 Schematic of the formation of nanocrystalline yttrium oxysulfide.

polysulfide (NH_4S_x) vapours. Nitrate sols of $Y_2O_3-Eu_2O_3$ trapped inside the organic cages of the urea–formaldehyde (UFR) polymer network are sulfurized by NH_4S_x vapours generated during the thermolysis reaction. The UFR network can serve both as an effective fuel for the combustion reaction and also as a dispersing medium for the formation of nanoceramic particles. The chemical purity of the nanocrystalline samples can be confirmed on comparison with the JCPDS standard file(s) corresponding to the bulk Y_2O_2S system (Fig. 2).

Furthermore, the experimental result that the presence of other polymers such as polyvinyl alcohol [$\{-CH_2CH(OH)-\}_n$] did not yield the oxysulfide phase again suggests the role of UFR leading to the formation of ammonium polysulfide (NH_4S_x) in the sulfurization process. Ammonium polysulfide (NH_4S_x) formation may be explained by the possible reaction of ammonia vapours liberated following the decomposition of UFR with sulfur vapour phase. The process of sol being trapped inside the organic cages and the sulfurization process following the sol–gel polymer pyrolysis can be schematized as given in Fig. 3. The chemical purity of the nanocrystalline samples prepared can be ascertained by comparison with the XRD pattern of bulk $Y_2O_2S : Eu^{3+}$ indexable under the space group $P\bar{3}m1$ (Fig. 2). Also from Table 1, it can be seen that the least squares refined crystallographic cell parameters for the bulk and nano oxysulfide samples are in good agreement.

3.2. Particle size and morphology

Fig. 4 depicts a TEM image of the pyrolysis product indicating polyhedral morphology for the fine particles obtained after the thermolysis reaction. Although this method has yielded

Table 1 Least squares refined unit cell parameters for bulk and nanocrystalline $Y_2O_2S : Eu^{3+}$ samples

System	$a/\text{\AA}$	$c/\text{\AA}$	Cell volume/ \AA^3	% deviation in cell volume from std.
Bulk $Y_2O_2S : Eu^{3+}$	3.7812 ± 0.0015	6.5801 ± 0.0106	81.4722	0.2829
Nano $Y_2O_2S : Eu^{3+}$	3.7771 ± 0.0024	6.5531 ± 0.0172	80.9621	0.9072
JCPDS std # 24-1424	3.7840	6.5890	81.7033	—

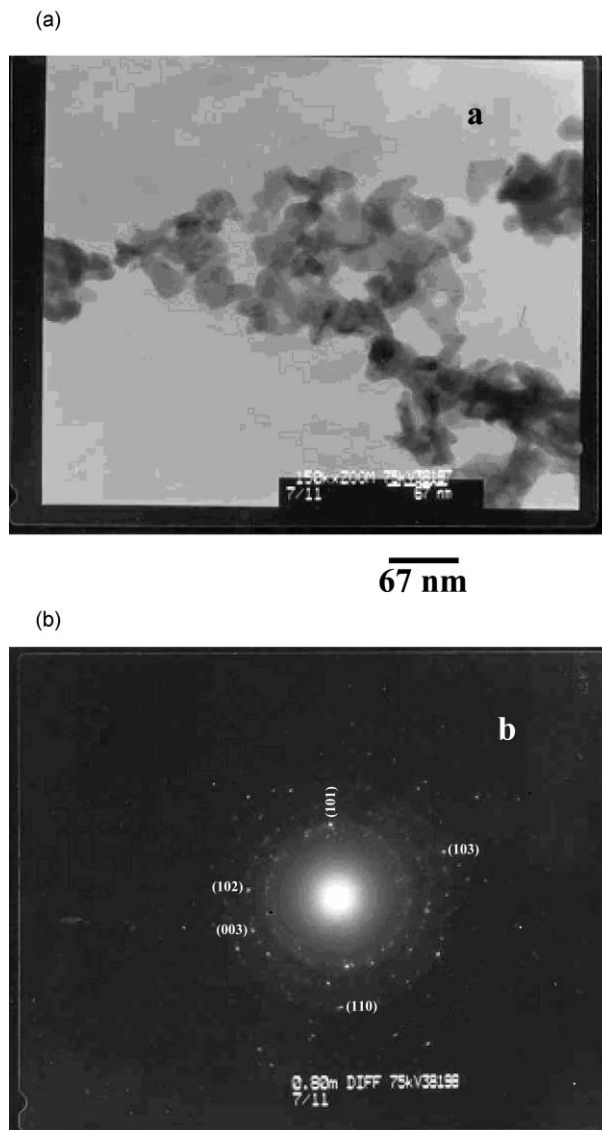


Fig. 4 (a) TEM image of nanocrystalline $\text{Y}_2\text{O}_2\text{S} : \text{Eu}^{3+}$. (b) The corresponding SAED pattern.

somewhat agglomerated particles, there are well dispersed particles having polyhedral morphology with an average diameter of about 20 ± 1 nm (Fig. 4a). This value is in good agreement with the particle size estimate made using X-ray diffraction line-broadening data in conjunction with the Scherrer formula which gave a value of 21 nm. The polyhedral morphology lacking any structural features observed for the crystallites obtained can be attributed to the two dimensional organic network of the urea-formaldehyde resin. The precursor sol gets distributed in these organic rings and on pyrolysis is converted to crystallites.

Furthermore, the selected area electron diffraction (SAED) pattern obtained for the corresponding area of the sample is consistent with a $\text{Y}_2\text{O}_2\text{S}$ phase (Fig. 4b). The spotty diffraction pattern comprising somewhat concentric circles suggests the presence of a polycrystalline $\text{Y}_2\text{O}_2\text{S}$ phase. However the SAED pattern also shows some weak spots corresponding to a Y_2O_3 phase which may be present as an impurity phase in traces. The presence of Y_2O_3 as an impurity phase may be attributed to incomplete sulfurization. This may be because sulfurization by over-coating of Y_2O_3 crystallites could not be completed during the course of the pyrolysis reaction. Alternatively, it is also probable that during the pyrolysis reaction, there might be some possibility of part of the $\text{Y}_2\text{O}_2\text{S}$ phase being reconverted to the Y_2O_3 phase. In any case, the presence of $\text{Y}_2\text{O}_3 : \text{Eu}^{3+}$ as

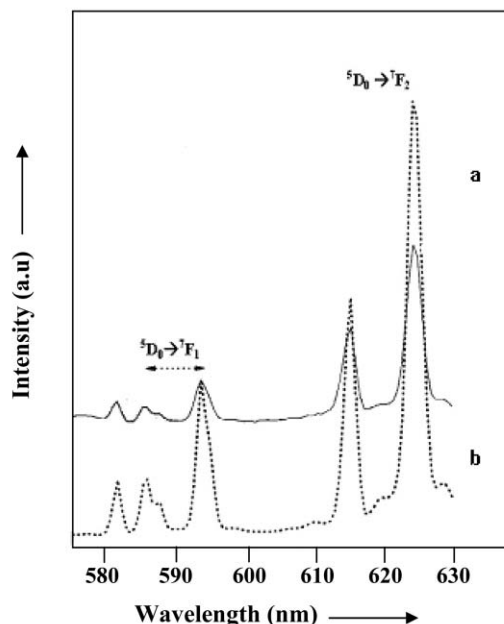


Fig. 5 Photoluminescence emission spectra of (a) bulk and (b) nanocrystalline $\text{Y}_2\text{O}_2\text{S} : \text{Eu}^{3+}$ samples (excitation was in the Eu^{3+} -ligand charge transfer band(s) in both cases).

an impurity phase can be ignored for all practical purposes. This is because these phases are so distinct in spectral characteristics that the presence of $\text{Y}_2\text{O}_3 : \text{Eu}^{3+}$ traces as an impurity phase may not affect the fluorescence properties of the nano $\text{Y}_2\text{O}_2\text{S} : \text{Eu}^{3+}$ phase.

3.3. Photoluminescence characteristics

The photoluminescence emission spectra (Fig. 5) measured under charge transfer excitation ($\lambda_{\text{exc}} = 320$ nm) show good comparison between the bulk and nanocrystalline $\text{Y}_2\text{O}_2\text{S} : \text{Eu}^{3+}$ samples. The sharp emission lines observed can be assigned to ${}^5\text{D}_0 \rightarrow {}^7\text{F}_J$ ($J = 0-2$) transitions arising from localized intra-configurational f-f transitions of Eu^{3+} . Identical Stark-splitting patterns observed in the ${}^5\text{D}_0 \rightarrow {}^7\text{F}_J$ levels for both bulk and nano samples suggest the same kind of cationic site(s) occupied by Eu^{3+} in both cases in terms of chemical coordination and symmetry. On the other hand there is a marked difference in the excitation spectra between the bulk and nanocrystalline samples. Based on the photo-excitation region, the excitation can be classified into two types, viz. (i) *excitonic* type for photo-excitations around the band edge region of the host matrix (Fig. 6) and (ii) *charge-transfer* type corresponding to the $\text{Eu}^{3+}-\text{O}^{2-}$ ($4f^7-2p^{-1}$) or S^{2-} electron transfer transitions (Fig. 7). For the bulk $\text{Y}_2\text{O}_2\text{S} : \text{Eu}^{3+}$ system, the charge-transfer excitation band occurs around 335 nm while the excitonic excitation corresponding to the band-edge region of the $\text{Y}_2\text{O}_2\text{S}$ host occurs at higher energy somewhere around 220–230 nm. It can be seen from Fig. 6 and 7 that the nanocrystalline sample shows substantial blue shifts of about 5000 cm^{-1} in the excitonic and about 2000 cm^{-1} in the charge transfer regions. In order to explain the blue-shifts observed, the contribution from the innumerable surface-states acquiring prominence, the modification in optical electronegativity and the allied features have to be considered.

From Jorgensen's empirical relation,¹⁸ the position of $\text{Eu}^{3+}-\text{O}^{2-}$ charge transfer band can be given by

$$\nu_{\text{CT}} = [\chi_{\text{opt}}(\text{X}) - \chi_{\text{uncorr}}(\text{M})] \times 30000 \text{ cm}^{-1} \quad (1)$$

with $\chi_{\text{opt}}(\text{X})$ and $\chi_{\text{uncorr}}(\text{M})$ respectively being the optical electronegativities of the ligand and central metal ion. Also we have from Jorgensen's refined electron spin pairing theory the

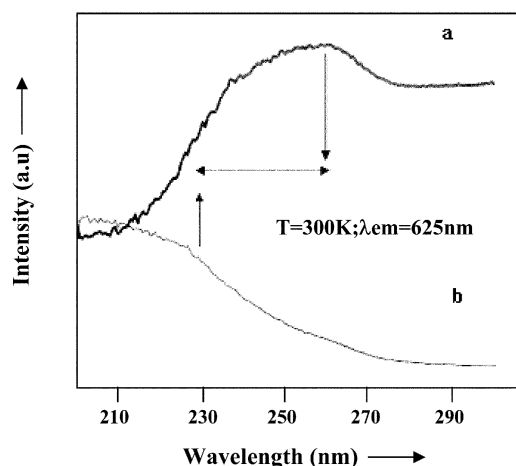


Fig. 6 Photoluminescence excitation spectra (corresponding to excitonic region) of (a) bulk and (b) nanocrystalline $Y_2O_2S : Eu^{3+}$ samples.

position of ligand to metal charge transfer band as

$$v_{CT} = W - q(E-A) + 1/13N(S)D + M(L)E^3 + P(S, L, J)\zeta_{4f} \quad (2)$$

where W is a constant zero point, $(E-A)$ is an empirical parameter accounting for stabilization of 4f electrons, D is the change in spin-pairing energy for the configurational change and q is the number of f-electrons or the charge (the remaining variables have been defined previously¹⁸).

In a nanocrystalline system, surface states arise from the lattice lacking periodicity, broken chemical bonds and so on. In the same way as for the nanocrystalline system we can explain the blue-shift observed in the charge transfer excitation band. In particular the spin-pairing energy term D may be considerably modified due to the presence of new surface states in the nanocrystals arising from broken $Eu^{3+}-O^{2-}/(S^{2-})$ bonds. This may influence the Eu^{3+} luminescence properties as described below.

From Table 2 we see that in the case of the oxysulfide nanocrystalline $Y_2O_2S : Eu^{3+}$ sample, the intensity ratio of the hypersensitive (structure and ligand dependent) ${}^5D_0 \rightarrow {}^7F_2$ transition with respect to the structure independent ${}^5D_0 \rightarrow {}^7F_1$ emission transition increases nearly two fold when compared with that of the bulk system. For the case of the nanocrystalline $Y_2O_3 : Eu^{3+}$ system there is no such substantial change in the relative intensity. In order to explain this we should consider the following possibilities: either a significant enhancement in the oscillator strength (hence the emission intensity) of the hypersensitive ${}^5D_0 \rightarrow {}^7F_2$ electric dipole transition (or) significant decrease (hence the emission intensity) of the magnetic dipole transition. It should be noted that the dopant Eu^{3+} ion, already in the bulk system, sits in a low symmetry (C_{3v}) acentric¹⁹ site which facilitates the admixture of odd parity terms. Furthermore, identical Stark splitting patterns implied from the emission spectra suggest similar cationic site symmetry and chemical surroundings for the Eu^{3+} site(s) in the nano and bulk Y_2O_2S systems. Hence we reject the former

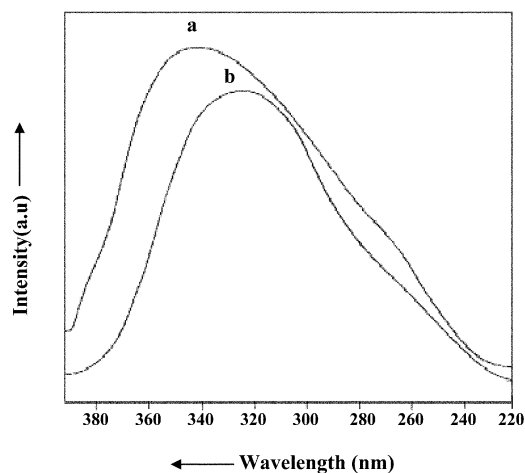


Fig. 7 Photoluminescence excitation spectra at the charge transfer region of (a) bulk and (b) nanocrystalline $Y_2O_2S : Eu^{3+}$ samples.

possibility of change in site-symmetry to account for this phenomenon. Instead the ${}^5D_0 \rightarrow {}^7F_1$ emission working by a magnetic dipole transition losing intensity appears to be a more plausible mechanism. However it is already known that a blue shift in the Eu^{3+} -ligand charge transfer band can lead to enhancement in the ${}^5D_0 \rightarrow {}^7F_2$ transition.²⁰

Notwithstanding these observations, there is an obvious size dependent shift in the position of the Eu^{3+} -ligand electron transfer absorption/excitation band. This, in our opinion, may stem from a possible size dependent change in covalency between the Eu^{3+} -ligand species located near the surface of the crystallites and hence optical electronegativity of the system.

Now turning to the excitonic excitation band, the experimentally observed blue-shift can be explained by the large bandgap semiconductor system showing a blue shift due to quantum confinement effects. Furthermore, the lower relative intensity observed for the hypersensitive transition may be related to possible non-radiative losses arising from surface states created in the nanocrystalline system.

4. Conclusions

Trivalent europium doped yttrium oxysulfide ($Y_2O_2S : Eu^{3+}$) nanoparticles of average size 20 nm have been prepared using a facile sol-gel pyrolysis route. In this synthesis, a urea-formaldehyde resin serving both as an organic fuel for the pyrolysis reaction and also as the dispersion matrix for the synthesis of the nanoceramic particles has been employed. Notwithstanding the similar coordination geometry of the ligand(s) surrounding the Eu^{3+} luminescent centre in the bulk and nano-oxysulfide systems, the latter shows a profound size dependent change in the photoluminescence excitation characteristics. Using the structure independent ${}^5D_0 \rightarrow {}^7F_1$ emission working by a magnetic dipole transition mechanism as the reference, the observed blue shift in the photoluminescence charge transfer excitation band has been explained as a possible size-dependent change in the optical electronegativity of the ligands surrounding the luminescent centre.

Table 2 Comparison of photoluminescent properties of bulk and nanocrystalline $Y_2O_2S : Eu^{3+}$ and $Y_2O_3 : Eu^{3+}$ samples ($T = 300$ K)

Sample	Particle size using TEM/SEM	Eu^{3+} -ligand (O^{2-}/S^{2-}) CTB max/nm	Excitonic band max/nm	Relative luminescence yield	Relative intensity of ${}^5D_0 \rightarrow {}^7F_2 / {}^5D_0 \rightarrow {}^7F_1$	
					Excitonic excitation	Charge transfer excitation
Bulk $Y_2O_2S : Eu^{3+}$	3 μm	335	260	100	3.5	8.4
Nano $Y_2O_2S : Eu^{3+}$	20 nm	320	240	12.7	0.2	15.7
Bulk $Y_2O_3 : Eu^{3+}$	3 μm	250	240	100	8.3	7.3
Nano $Y_2O_3 : Eu^{3+}$	20 nm	250	230	39.13	8.6	6.7

Acknowledgements

J. D. gratefully acknowledges the Director, CECRI, for all the research facilities provided and CSIR, India for the award of a Senior Research Fellowship.

References

- 1 D. K. Williams, B. Bihari, B. M. Tissue and J. M. McHale, *J. Phys. Chem. B*, 1998, **102**, 916.
- 2 B. Bihari, H. Eilers and B. M. Tissue, *J. Lumin.*, 1997, **75**, 1.
- 3 P. Yu, Z. K. Tang, G. K. L. Wong, M. Kawasaki, A. Ohtomo, H. Koinuma and Y. Segawa, *Proc. of 23rd Intl. Conf. on Physics of Semiconductors*, ed. M. Scheffler and R. Zimmermann Berlin, World Scientific, Singapore, 1996, vol. 2, p. 1453.
- 4 P. Yu, Z. K. Tang, G. K. L. Wong, M. Kawasaki, A. Ohtomo, H. Koinuma and Y. Segawa, *Solid State Commun.*, 1997, **103**, 459.
- 5 D. M. Bagnall, Y. F. Chen, Z. Zhu, T. Yao, S. Koyama, M. Y. Shen and T. Goto, *Appl. Phys. Lett.*, 1997, **70**, 2230.
- 6 T. Makino, T. Yasuda, Y. Segawa, A. Ohtomo, K. Tamura, M. Kawasaki and H. Koinuma, *Appl. Phys. Lett.*, 2001, **79**, 1282.
- 7 M. R. Royce and A. L. Smith, *Electrochem. Soc. Extd. Abstr.*, 1968, **34**, 94.
- 8 W. Rossner, M. Ostertag and F. Jermann, *Phys. Chem. Lumin. Mater.—Proc. Electrochem. Soc.*, 1998, **98–24**, 187.
- 9 S. H. Cho, J. S. Yoo and J. D. Lee, *J. Electrochem. Soc.*, 1998, **145**, 1017.
- 10 J. S. Yoo and J. D. Lee, *J. Appl. Phys.*, 1997, **81**, 2910.
- 11 M. Mikami and A. Oshiyama, *Phys. Rev. B*, 1998, **57**, 8939.
- 12 *Kirk-Othmer Encyclopedia of Chemical Technology*, 4th edn., Wiley-Interscience, New York, 1991, vol. 2.
- 13 K. Suresh, N. R. S. Kumar and K. C. Patil, *Adv. Mater.*, 1991, **3**, 148; S. S. Manoharan and K. C. Patil, *J. Am. Ceram. Soc.*, 1992, **75**, 1012.
- 14 M. R. Royce, *US Pat.* 3418246, 1968; P. N. Yocom, *US Pat.* 3418247, 1968.
- 15 B. D. Cullity, *Elements of X-Ray Diffraction*, Addison-Wesley, Menlo Park, CA, 1956.
- 16 J. Dhanaraj, R. Jagannathan, T. R. N. Kutty and Chung-Hsin Lu, *J. Phys. Chem. B*, 2001, **105**, 11098.
- 17 L. Ozawa, *J. Electrochem. Soc.*, 1977, **124**, 413.
- 18 C. K. Jorgensen, *Prog. Inorg. Chem.*, 1970, **12**, 101.
- 19 B. Saubat, C. Fouassier, P. Hagenmuller and J. Bourcet, *Mater. Res. Bull.*, 1981, **16**, 193.
- 20 G. Blasse, *Struct. Bonding*, 1976, **26**, 43.